

Decoupling H₂(g) and O₂(g) Production in Water Splitting by a Solar-Driven V₃+/₂+(aq,H₂SO₄)|KOH(aq) Cell

Alec Ho, Xinghao Zhou, Lihao Han, Ian Sullivan, Christoph Karp, Nathan Lewis, and Chengxiang Xiang

ACS Energy Lett., **Just Accepted Manuscript** • DOI: 10.1021/acsendergylett.9b00278 • Publication Date (Web): 21 Mar 2019

Downloaded from <http://pubs.acs.org> on March 21, 2019

Just Accepted

“Just Accepted” manuscripts have been peer-reviewed and accepted for publication. They are posted online prior to technical editing, formatting for publication and author proofing. The American Chemical Society provides “Just Accepted” as a service to the research community to expedite the dissemination of scientific material as soon as possible after acceptance. “Just Accepted” manuscripts appear in full in PDF format accompanied by an HTML abstract. “Just Accepted” manuscripts have been fully peer reviewed, but should not be considered the official version of record. They are citable by the Digital Object Identifier (DOI®). “Just Accepted” is an optional service offered to authors. Therefore, the “Just Accepted” Web site may not include all articles that will be published in the journal. After a manuscript is technically edited and formatted, it will be removed from the “Just Accepted” Web site and published as an ASAP article. Note that technical editing may introduce minor changes to the manuscript text and/or graphics which could affect content, and all legal disclaimers and ethical guidelines that apply to the journal pertain. ACS cannot be held responsible for errors or consequences arising from the use of information contained in these “Just Accepted” manuscripts.

1
2
3
4 Decoupling H₂(g) and O₂(g) Production in Water
5
6
7 Splitting by a Solar-Driven
8
9 V^{3+/2+}(aq,H₂SO₄)|KOH(aq) Cell
10

11 *Alec Ho¹, Xinghao Zhou², Lihao Han¹, Ian Sullivan¹, Christoph Karp¹, Nathan S. Lewis^{1, 3, 4*},*

12
13
14 *Chengxiang Xiang^{1*}*
15
16
17

18 ¹ Division of Chemistry and Chemical Engineering, California Institute of Technology, Pasadena, CA
19
20 91125, USA
21
22

23 ² Division of Engineering and Applied Science, Department of Applied Physics and Materials Science,
24
25 California Institute of Technology, Pasadena, CA 91125, USA
26
27

28 ³ Beckman Institute Molecular Materials Research Center, California Institute of Technology, Pasadena,
29
30 CA 91125, USA
31
32

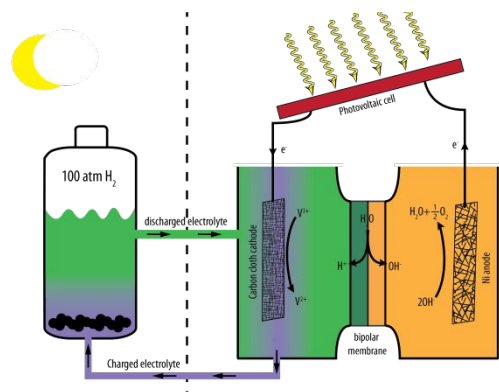
33 ⁴ Kavli Nanoscience Institute, California Institute of Technology, Pasadena, CA 91125, USA
34
35
36
37
38
39
40
41
42
43
44
45
46
47
48

49 *To whom correspondence should be addressed: nslewis@caltech.edu, cxx@caltech.edu
50
51
52
53
54
55
56
57
58
59
60

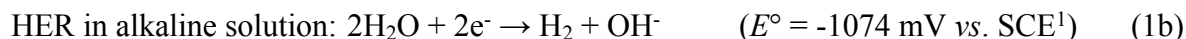
ABSTRACT

1
2
3
4
5
6
7 A solar-driven $V^{3+/2+}(\text{aq}, \text{H}_2\text{SO}_4)|\text{KOH}(\text{aq})$ cell, consisting of a carbon-cloth cathode in 2.0 M
8
9 $\text{H}_2\text{SO}_4(\text{aq})$ with 0.36 M $\text{V}_2(\text{SO}_4)_3$ (pH = -0.16), a Ni mesh anode in 2.5 M $\text{KOH}(\text{aq})$ (pH = 14.21)
10
11 for the oxygen-evolution reaction (OER), and a bipolar membrane that sustained the pH
12
13 differentials between the catholyte and anolyte, enabled water splitting with spatial and temporal
14
15 decoupling of the hydrogen-evolution reaction (HER) from the OER and produced $\text{H}_2(\text{g})$ locally
16
17 under pressure upon demand. Over a range of potentials and charging depths, V^{3+} was selectively
18
19 reduced with > 99.8% Faraday efficiency (FE). The V^{2+} species produced in the catholyte was
20
21 then passed subsequently on demand over a MoC_x -based HER catalyst to produce $\text{H}_2(\text{g})$ and
22
23 regenerate V^{3+} for subsequent reduction. Under a base hydrogen pressure of 1 atm, 10 atm and
24
25 100 atm, the discharge efficiency of the V^{3+} to hydrogen was 83%, 65.2% and 59.8%, respectively.
26
27 In conjunction with a solar tracker and a photovoltaic device, the $V^{3+/2+}(\text{aq}, \text{H}_2\text{SO}_4)|\text{KOH}(\text{aq})$ cell
28
29 was charged outdoors under sunlight and discharged at night with a daily averaged diurnal solar-
30
31 to-hydrogen (STH) energy conversion efficiency of 3.7% and a STH conversion efficiency of 5.8%
32
33 during daylight operation.
34
35
36
37
38
39
40
41
42
43
44
45
46
47
48
49
50
51
52
53
54
55
56
57
58
59
60

TOC GRAPHICS



In a solar-driven water-splitting electrochemical cell, the hydrogen-evolution reaction (HER) occurs at the cathode while the oxygen-evolution reaction (OER) occurs at the anode:



where SCE is the standard calomel electrode in saturated KCl. In a photot electrochemical (PEC) cell, reaction (1) and reaction (2) are tightly coupled, and to insure charge neutrality, must proceed at the same rate.²⁻⁵ Hence, most solar-driven water-splitting cells, operated either under conventional single-electrolyte conditions,⁵⁻⁶ or in electrolytes that have sustained pH differentials between the catholyte and anolyte,³⁻⁴ generate H₂(g) and O₂(g) simultaneously in the cell, so that whenever one oxygen molecule is produced at the anode, two hydrogen molecules are produced at the cathode. H₂(g)/O₂(g) mixtures have a flammability limit of 4 vol.% and an explosive limit of 15 vol.%,⁷ so, for safety purposes, membrane separators such as a cation-exchange membrane (CEM), *e.g.*, Nafion, an anion-exchange membrane (AEM), *e.g.*, Selemion, or a bipolar membrane (BPM), *e.g.*, Fumasep, are often used to support ionic transport and prevent gaseous-product crossover.²⁻³ Membrane-free devices lack a robust mechanism to prevent product-gas crossover, and in some measurements, up to 40% of H₂ is present in the O₂-containing anolyte chamber⁸ but in some cases strategies have been developed to separate the products under 1 atm of pressure with low crossover rates.⁹⁻¹⁰ The membrane separator also facilitates the production of H₂(g) under pressure by electrochemical processes.¹¹⁻¹²

1
2
3
4
5
6
7 Membrane separators provide an effective method to minimize product crossover, but mechanical
8
9 failures and pinhole formation in the membrane introduce safety concerns.¹³⁻¹⁴ Additionally, such
10
11 an approach necessitates a balance-of-systems for collection of the evolved H₂(g) over large areas
12
13 as well as pressure management technologies associated with accommodating the time-varying
14
15 instantaneous intensity of sunlight striking the system at different spatial locations.^{2-3, 6} An
16
17 approach that enabled the separate generation of hydrogen and oxygen in space and time would
18
19 thus entail several advantages, including mitigating the concern related to production of potentially
20
21 flammable or explosive gas mixtures. In such an approach, the hydrogen generation rate could also
22
23 beneficially be decoupled from, and thus could substantially exceed, the rate of generation of
24
25 energetic electrons and holes in the illuminated light absorbers. Furthermore, the H₂ could be
26
27 formed upon demand under pressure at a specific desired location. A benign aqueous solution
28
29 could constitute the redox catholyte material collected over the large solar-illuminated area and
30
31 serve as the collected energy carrier, with the O₂(g) produced in place and vented to the atmosphere
32
33 without the presence of H₂(g) at that location.
34
35
36
37
38
39
40
41
42
43
44

45 Two general strategies have been used to decouple the HER and OER electrochemically and/or
46
47 photoelectrochemically. The first strategy involves a two-step electrolysis, in which the water-
48
49 splitting reaction is effected in two physically distinct, separate electrochemical cells, using redox
50
51 species or redox electrodes such as NiOOH electrodes,¹⁵⁻¹⁶ a polytriphenylamine-based battery
52
53 electrode,¹⁷ or molecular electron-coupled-proton buffers.¹⁸⁻¹⁹ The second strategy to decouple the
54
55
56
57
58
59
60

1
2
3
4 generation of hydrogen and oxygen involves a (photo-)electrochemical process in conjunction with
5
6 a subsequent chemical process, using for example silicotungstic acid,²⁰ vanadium or cerium redox
7
8 couples²¹ as electrochemical mediators to couple two electrochemical processes and allow
9
10 completion of a sustainable, complete water-splitting process.
11
12
13

14
15
16
17 Herein, we demonstrate such a spatially and temporally decoupled approach to solar-driven
18
19 electrochemical water-splitting, in which the electrons and protons generated during the OER are
20
21 used to charge an aqueous $V^{3+/2+}$ (aq) solution in 2.0 M sulfuric acid (pH = -0.16) (Reaction 3),
22
23 rather than being used directly to produce H_2 (g) at the cathode. The protons produced at the anode
24
25 are transported to the catholyte and temporarily stored in the catholyte, which causes the decrease
26
27 of the catholyte pH during the charging process.
28
29
30



32
33
34
35 To produce H_2 (g) from water, the catholyte that contains the V^{2+} is then exposed upon demand, if
36
37 desired at a separate location and time, to a catalyst in the dark. During the chemical discharging
38
39 process, the pH of the catholyte increases back to its initial value upon the release of hydrogen. In
40
41 the demonstration system developed herein, the charged vanadium solution V^{2+} is specifically
42
43 contacted with a Mo_2C catalyst, resulting in the production of H_2 (g) and V^{3+} (Reaction 4).
44
45
46



48
49
50
51 The full cell, and thus the overall water-splitting process, is completed with the evolution of O_2 (g)
52
53 from water at the anode, as per equation (2a) or (2b).
54
55
56
57
58
59
60

1
2
3
4 The $V^{3+/2+}$ redox couple is however only soluble in acidic conditions, in which a stable, active,
5
6 earth-abundant OER catalyst has yet to be discovered.²²⁻²³ A range of OER catalysts composed of
7
8 binary, ternary or quaternary metal oxides exhibit low overpotentials and high stabilities in alkaline
9
10 conditions.²⁴⁻²⁷ To simultaneously accommodate the optimal pH conditions for the OER and
11
12 vanadium redox reactions, a bipolar membrane has thus been used in the demonstration system
13
14 discussed herein, to sustain the pH differential between the cathode and the anode chamber under
15
16 steady-state operation in the cell as well as to enable the use of earth-abundant electrocatalysts in
17
18 a system that produces $H_2(g)$ locally under pressure and upon demand. Fig.S1 shows a schematic
19
20 illustration of the full process flow.
21
22
23
24
25
26
27
28
29

30 Fig. 1 shows a schematic illustration of the solar-driven $V^{3+/2+}(aq, H_2SO_4)|KOH(aq)$ system, which
31
32 for proof-of-concept purposes consisted of a series connection between a photovoltaic module and
33
34 an electrochemical cell. The 16.0% efficient polycrystalline Si photovoltaic module produced the
35
36 photovoltage and photocurrent necessary to drive the electrochemical reactions, although an
37
38 analogous process could occur in an integrated system that used instead a photoelectrode either as
39
40 the anode, cathode, or both.²⁸⁻³⁰ For example, in conjunction with appropriately selected
41
42 photoanodes, p-InP and p-Si could be used in an integrated system, since both materials provide
43
44 stable photocathodes in contact with $V^{3+/2+}(aq)-HCl(aq)$ with p-InP exhibiting >11% efficiency
45
46 under such conditions.³¹ A carbon cloth electrode effected the reduction of vanadium in 2.0 M
47
48 H_2SO_4 (pH=-0.16), with an initial $[V^{3+}] = 0.36$ M; a Ni mesh electrode performed the OER in 2.5
49
50 M KOH (pH=14.21); and a bipolar membrane sustained the pH differentials and provided protons
51
52
53
54
55
56
57
58
59
60

1
2
3
4 and hydroxide ions to the catholyte and anolyte, respectively.
5
6
7

8
9 The electrochemical behaviors of the cathode, anode and the bipolar membrane have been
10 evaluated separately (Fig. 2). Fig. 2a shows the linear sweep voltammetry, at a scan rate of 40 mV
11 s⁻¹, of a Ni mesh electrode in 2.5 M KOH(aq) (pH = 14.21) (red) and of a Pt foil electrode in 1.0
12 M H₂SO₄(aq) (blue). Under these conditions, an overpotential of 379 mV, i.e. a potential of 539
13 mV *vs.* SCE was required for the Ni mesh to drive the OER at an anodic geometric current density
14 of 10 mA cm⁻². The relatively low current density, 10 mA cm⁻², was chosen for evaluating the
15 catalyst and cell performance due to the relatively low photon flux from sunlight for the potential
16 usage of this proof-of-concept device in a distributed system. Fig. 2b shows the voltammetry, at a
17 scan rate of 40 mV s⁻¹, of a carbon cloth electrode in a 2.0 M H₂SO₄(aq) with (green) and without
18 0.36 M V₂(SO₄)₃ (black). A potential of -765 mV *vs.* SCE, i.e. an overpotential of -266 mV relative
19 to $E^{\circ}(\text{V}^{3+}/2^{+})$, was required to drive the V³⁺ reduction at a cathodic geometric current density of
20 10 mA cm⁻². In contrast, at the same current density in the pure 2.0 M H₂SO₄(aq) solution, a
21 potential of -858 mV *vs.* SCE, i.e. an overpotential of -614 mV, was required to drive the HER.
22 During the vanadium redox charging process, HER is a parasitic side reaction, which is suppressed
23 due to the slow kinetics for the HER at carbon cloth electrodes.
24
25
26
27
28
29
30
31
32
33
34
35
36
37
38
39
40
41
42
43
44
45
46
47
48
49
50

51 The polarization behaviors of the bipolar membrane that sustained the pH differentials between
52 the catholyte and anolyte with or without the vanadium redox couples were measured absence of,
53 and then in the presence of, the vanadium redox couples. Fig. 2c shows the voltage drop measured
54
55
56
57

1
2
3
4 with a four-point configuration across the bipolar membrane, as a function of the current density
5
6 normalized to the area of the bipolar membrane. The grey polarization curve represents the
7
8 electrolyte combination of KOH(aq) (pH = 14.21) and 2.0 M H₂SO₄(aq) (pH = -0.16) without the
9
10 vanadium redox species. A slight decrease in the voltage loss was observed when 0.36 M V₂(SO₄)
11
12 was added to the catholyte (black polarization curve, Fig. 2c), likely due to the increased the
13
14 conductivity of the solution due to the presence of additional electrolyte. At open-circuit, the
15
16 equilibrium potential drop, $V_{\text{membrane, equilibrium}}$ was $0.059 \times (14.21+0.16) = 0.848 \text{ V}$. At a current
17
18 density of 10 mA cm^{-2} , the potential difference across the bipolar membrane was 0.866 V in the
19
20 presence of V^{3+/2+}. The bipolar membrane voltage loss at 10 mA cm^{-2} was therefore $V_{\text{membrane, loss}}$
21
22 $= V_{\text{membrane, total}} - V_{\text{membrane, equilibrium}} = 0.866 \text{ V} - 0.848 \text{ V} = 0.018 \text{ V}$. The observed current voltage
23
24 characteristic of the bipolar membrane at two extreme pH values is in agreement with prior
25
26 reports,³²⁻³³ and is substantially lower than voltage losses across bipolar membranes operated in
27
28 near-neutral pH conditions.^{3, 33-36} Table S1 summarized the voltage losses in the reported bipolar
29
30 membrane systems. At two extreme pHs, the minimal voltage loss across the bipolar membrane,^{33,}
31
32 ³⁷ is consistent with the hypothesis that no additional Donnan potential drop is present across the
33
34 membrane/electrolyte interface, and all the electric field drops primarily occur at the CEM and
35
36 AEM interface. The voltage stability as well as the crossover properties of the bipolar membrane
37
38 was also measured. Fig. 2d shows the voltage measured across the bipolar membrane as a function
39
40 of time, when the 0.36 M V₂(SO₄)₃, 2.0 M H₂SO₄(aq) (pH = -0.16) / bipolar membrane / 2.5 M
41
42 KOH(aq) (pH = 14.21) cell was biased at a constant current density of 10 mA cm^{-2} . These data
43
44 indicated negligible degradation in the voltage across the bipolar membrane over the course of a
45
46
47
48
49
50
51
52
53
54
55
56
57
58
59
60

200 h stability test. For > 200 h, the bipolar membrane remained stable, and no precipitate was observed either in the bipolar membrane or in the anolyte. The geometric surface areas of the bipolar membrane, carbon cathode, and nickel mesh anode were all 6.0 cm². To study the ion crossover behaviors, the concentrations of V^{3+/2+} in the anolyte before and after continuous operation at 10 mA cm⁻² for 24 h were determined using inductively coupled plasma mass spectroscopy (ICP-MS, Table S2), and the concentrations of K⁺ in the catholyte and SO₄²⁻ in the anolyte were determined using ion chromatography (IC). Table 1 lists the transport current density corresponding to the leakage of V^{3+/2+}, K⁺ and SO₄²⁻ across the membrane when the cell was operated at 10 mA cm⁻². The membrane selectivity in the absence of and then in the presence of vanadium species, determined by the ratio of the proton-carried and hydroxide-carried portions of the total passed charges, f_{H^+} and f_{OH^-} , is also summarized in Table 1. The V^{3+/2+} crossover current density was negligible partly due to the electric field lines during the cell operation repelling the positively charged vanadium redox species from entering the bipolar membrane and the anolyte. The presence of V^{3+/2+} also did not substantially affect membrane selectivity. Both the f_{H^+} and f_{OH^-} values exceeded 92% at an operating current density of 10 mA cm⁻², in accord with prior results.³

Table 1. Ion crossover rates for the bipolar membrane in the absence of and then in the presence of vanadium ions

$J_{\text{Membrane}} = 10 \text{ mA cm}^{-2}$	$J_{V^{3+/2+}}$	J_{K^+}	$J_{SO_4^{2-}}$	f_{H^+}	f_{OH^-}
---	-----------------	-----------	-----------------	-----------	------------

With $V^{3+/2+}$	0.226 $\mu\text{A cm}^{-2}$	787 $\mu\text{A cm}^{-2}$	54 $\mu\text{A cm}^{-2}$	92.1%	99.5%
Without $V^{3+/2+}$	N.A.	606 $\mu\text{A cm}^{-2}$	184 $\mu\text{A cm}^{-2}$	93.9%	98.2%

The electrochemical charging and discharging behaviors of the carbon cloth electrode in $V^{3+/2+}$, 2.0 M $\text{H}_2\text{SO}_4(\text{aq})$ were then investigated. Fig. 3a shows the experimental (red) and theoretical (blue) decay of the current density with respect to charge passed into a 0.36 M $\text{V}_2(\text{SO}_4)_3$, 2.0 M H_2SO_4 solution. To obtain the current density ascribable to V^{3+} reduction (Fig. 3a, red), the current density that effected $\text{H}_2(\text{g})$ production (black) was subtracted from the overall current density, with the average $\text{H}_2(\text{g})$ -related current density over 30 min intervals calculated by measurement of the amount of $\text{H}_2(\text{g})$ collected with respect to charge passed. The decrease in current density as a function of charge passed followed the trend expected from the Nernst relation (Equation 5), where k is Boltzmann's constant, T is the absolute temperature, e is the unsigned charge on an electron, E is the Nernstian cell potential, $E^{o'}$ is the formal potential, [Red] is the concentration of reduced species and [Ox] is the concentration of oxidized species.

$$E = E^{o'} - \frac{kT}{q} \ln \frac{[\text{Red}]}{[\text{Ox}]} \quad (5)$$

The initial rapid decay of the current density was due to the rapid change of $E(V^{3+/2+})$ (Equation 2). As $[V^{3+}]$ decreased and $[V^{2+}]$ increased linearly as a function of the charge passed, the Nernstian cell potential shifted logarithmically to more negative values, consistent with the observed decreases in the charging current (Fig. 3a). The pH of the catholyte, an aqueous $V^{3+/2+}(\text{aq})$ solution in 2.0 M sulfuric acid, of the hybrid solar-driven water-splitting system decreased during the charging process and increased back to its initial value during the discharging process. The change

1
2
3
4 of the pH in the reported system is small (from -0.16 to -0.30) due to the large concentration
5
6 differential between the redox species and the sulfuric acid, and consequently the pH change had
7
8 minimal effects on the catalytic activities of the redox species or on the efficiency of the device.
9

10
11
12
13
14 Fig. 3b shows the collected $\text{H}_2(\text{g})$ as a function of the charge passed for the carbon cloth cathode
15
16 at -730 mV (purple), -830 mV (green), and -1000 mV (blue) vs. SCE, respectively, in 0.36 M
17
18 $\text{V}_2(\text{SO}_4)_3$, 2.0 M $\text{H}_2\text{SO}_4(\text{aq})$. Before the charging capacity of the electrolyte was reached at each
19
20 different potential, negligible $\text{H}_2(\text{g})$ was produced during charging of the 50.0 mL $\text{V}^{3+/2+}(\text{aq})$
21
22 solution. In contrast, as expected, a linear increase of the collected $\text{H}_2(\text{g})$ production (red) as a
23
24 function of the charge passed was observed for the same carbon cloth electrode in the blank 2.0 M
25
26 $\text{H}_2\text{SO}_4(\text{red})$ (dotted black line). For the carbon cloth electrode at -830 mV or at -1000 mV vs. SCE,
27
28 after the vanadium electrolyte reached its charging capacity, a rapid switch to $\text{H}_2(\text{g})$ production
29
30 was observed, with a rate of $\text{H}_2(\text{g})$ generation matching the theoretical value. When the carbon
31
32 cloth electrode was poised at -730 mV vs. SCE, an increase in the rate of $\text{H}_2(\text{g})$ production began
33
34 at ~83% of the $\text{V}^{3+/2+}$ charging capacity. The operating current density decreased substantially, to
35
36 ~ 0 mA cm^{-2} , for the low-overpotential condition (-730 mV vs. SCE), whereas before reaching its
37
38 charging capacity (see Fig. S2), the operating cathodic current density remained above ~0.8 mA
39
40 cm^{-2} and ~2.5 mA cm^{-2} for the high-overpotential conditions, -830 mV and -1000 mV, respectively.
41
42 Hence, during charging, the shifts in the equilibrium potential for the vanadium electrolyte resulted
43
44 in the decrease in operating current density (Fig. 3a), and decreased the selectivity towards
45
46 vanadium reduction. To achieve near-unity Faraday efficiency (FE) for vanadium reduction, an
47
48
49
50
51
52
53
54
55
56
57
58
59
60

1
2
3
4 overpotential of 331 mV, or a potential of -830 mV *vs.* SCE, was required during the reaction.
5
6
7

8
9 The collected H₂(g) as a function of the charge passed for the carbon cloth electrode at -830 mV
10
11 *vs.* SCE, at three different charging depths, is presented in Fig. 3c. The carbon cloth electrode
12
13 exhibited near-unity *FE* for vanadium reduction at charge capacities of 27% (orange), 55% (blue),
14
15 and 96% (black), as well as past 100% (green). The highly selective reduction of V³⁺ to V²⁺,
16
17 relative to H₂(g) formation, resulted from the competition between the thermodynamic potential
18
19 of the HER and the kinetic overpotential for vanadium reduction. Although at pH = -0.16, *E*^o
20
21 (H⁺/H₂) is 255 mV > *E*^o(V^{3+/2+}), carbon cloth is a poor electrocatalyst for the HER, leading to
22
23 near-unity *FE* for the vanadium reduction even at potentials substantially more negative than *E*^o
24
25 (H⁺/H₂). In addition, the HER was suppressed substantially when the electrode was biased at the
26
27 same potential (-830 mV *vs.* SCE) in the electrolyte with the presence of vanadium redox couples
28
29 (Fig. 2b). From the voltammetric behavior (the black and the green curve in Fig. 2b) of the
30
31 electrodes, the differential current densities at -830 mV *vs.* SCE suggest only ~40% *FE* for
32
33 vanadium reduction, however, near-unity *FE* was observed at various charging conditions. The
34
35 absorption of vanadium species at the carbon cloth electrode is likely to play a role in suppressing
36
37 the HER. During the entire charging process, the expected pH changes were observed in the
38
39 catholyte. The stored reducing equivalents in V²⁺ can however be rapidly and efficiently converted
40
41 into H₂(g) by the Mo₂C catalyst (see Fig. S4 for experimental setup). Accordingly, H₂(g)
42
43 production efficiencies (based on the total amount of charge passed) of 87%, 87% and 83% were
44
45 observed for vanadium solutions that were charged to 27%, 55% and 96% of their charging
46
47
48
49
50
51
52
53
54
55
56
57
58
59
60

1
2
3
4 capacity, respectively (Fig. 3d), when the produced H₂(g) was vented to the atmosphere. The H₂(g)
5
6 production efficiencies were defined by the following equation:
7

$$\eta_{H_2} = \frac{nF(V_{\text{collected_H}_2}/V_m)}{Q} \quad (6)$$

8
9
10
11 where n is the number of electrons, F is Faraday's constant, $V_{\text{collected_H}_2}$ is the volume of the
12 collected H₂ (mL), V_m is the molar volume of gas and Q is the total quantity of electric charge
13
14
15
16
17
18
19
20
21
22
23
24
25
26
27
28
29
30
31
32
33
34
35
36
37
38
39
40
41
42
43
44
45
46
47
48
49
50
51
52
53
54
55
56
57
58
59
60
passed during the charging process. The Mo₂C catalyst can be readily filtered through the
discharged electrolyte, facilitating catalyst recycling and reuse.

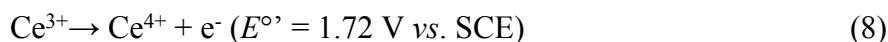
Discharging of the V²⁺ electrolyte was also performed under elevated pressures in a pressurized
stainless-steel apparatus (Fig. S5 and Fig. S6). The apparatus consisted of 10.4 mL of headspace
and 25.0 mL of fully charged V²⁺ electrolyte, as well as the Mo₂C catalyst. The pressure of the
headspace was equilibrated at 10.0 atm or at 100.0 atm with hydrogen gas. Upon contact of the
charged V^{3+/2+} solution with the Mo₂C catalyst, the pressure of the headspace increased rapidly,
due to the production of H₂(g). At 10.0 atm and 100.0 atm base pressure, the discharge of the V²⁺
electrolyte increased the pressure of the headspace by 6.65 atm and 5.97 atm, respectively,
corresponding to H₂(g) production efficiencies of 65.2% and 59.8%, respectively.

The electricity-to-fuel conversion efficiency of the bipolar membrane-based hybrid system (Table
2, System C), in which the cathode operated in an acidic solution for vanadium reduction and the
anode effected the OER in an alkaline electrolyte, was compared to the behavior of two previously
reported systems (Table 2, System A or System B) for hydrogen production at 1 atm. The

electricity-to-fuel conversion efficiency of those systems was defined by the following equation:

$$\eta_{\text{electricity-to-fuel}} = \frac{V_{\text{thermodynamic}}}{V_{\text{operating}}} \quad (7)$$

System A is a conventional, direct water-splitting reactor in 1.0 M H₂SO₄(aq), in which the Pt cathode and the IrO_x anode are separated by a Nafion membrane. System B consists of a previously reported indirect water-splitting reactor in which the carbon cloth cathode for vanadium reduction and a Pt anode for Ce oxidation (Reaction 8) are separated by a Nafion membrane, with the anolyte and catholyte both at the same pH, i.e. 1.0 M H₂SO₄(aq).²¹



In system B, the reduced vanadium electrolyte and the oxidized cerium electrolyte can be discharged separately to produce H₂(g) (Reaction 4) and O₂(g) (Reaction 9), respectively.²¹

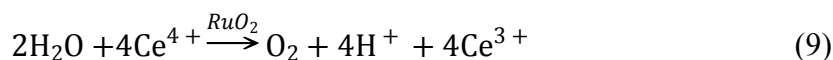


Table 2 presents the total voltage required for operation under thermodynamic limit for each of the three systems under consideration. The value of $E^{\circ}(\text{V}^{3+/2+})$ is 255 mV more negative than $E^{\circ}(\text{H}^+/\text{H}_2)$, whereas $E^{\circ}(\text{Ce}^{4+/3+})$ is 490 mV more positive than $E^{\circ}(\text{O}_2/\text{H}_2\text{O})$. Hence, at the thermodynamic limit, the required voltage for System B is 745 mV larger than for System A, and the required voltage for System C is 255 mV more than for System A. Assuming that H₂(g) under standard conditions is the final product for all three systems, the ideal electricity-to-hydrogen conversion efficiencies, for System B and System C are therefore $1.230 \text{ V} / 1.698 \text{ V} = 72 \%$, and $1.230 \text{ V} / 1.488 \text{ V} = 83\%$, respectively.

1
2
3
4
5
6
7 To facilitate comparisons between the three systems operating under realistic conditions, Fig. 2
8
9 also displays the behavior of a state-of-the-art Pt electrode for the HER as well as for the oxidation
10
11 of Ce^{3+} oxidation in acid. The state-of-the-art Pt electrode (grey curve in Fig. 2b) exhibited a small
12
13 overpotential (37 mV) at a current density of -10 mA cm^{-2} for the HER. The larger overpotential
14
15 for V^{3+} reduction at the carbon-cloth electrode (266 mV at -10 mA cm^{-2} , see Table S3) relative to
16
17 the state-of-the-art HER performance at Pt produces a loss in efficiency in this indirect solar-driven
18
19 water-splitting system and is likely due to the electrolyte resistive loss in a large geometric area
20
21 electrode (6.0 cm^2) operating at high currents, which could be further minimized through cell
22
23 engineering. To drive cerium oxidation (Reaction 5) at 10 mA cm^{-2} (blue curve in Fig. 2a) at Pt, a
24
25 potential of 1684 mV vs. SCE, i.e. an overpotential of 244 mV, was required. These overpotentials
26
27 (see Table S3) yield practical electricity-to-hydrogen conversion efficiencies for System B and
28
29 System C of 52% and 54%, respectively. In addition to the higher attainable electricity-to-fuel
30
31 conversion efficiency, System C also mitigates the need for noble-metal catalysts, such as RuO_2
32
33 in a heated environment, which also entails limited stability for oxygen generation from the Ce^{4+}
34
35 solution.²¹ Note that these efficiency values include losses associated with a lack of equilibration
36
37 of H_2 under pressure with the charged vanadium solution, but neglect the generally small losses
38
39 associated with energy required to circulate the electrolyte.
40
41
42
43
44
45
46
47
48
49
50
51
52

53 **Table 2.** Comparison of conversion efficiencies of three different systems
54
55
56
57
58
59
60

	System A	System B	System C
Thermodynamic voltage	1.230 V	1.698 V	1.488 V
Ideal conversion efficiency	100%	72%	83%
Realistic conversion efficiency	72%	52%	54%

System A: Pt/1.0 M H₂SO₄/Nafion/1.0 M H₂SO₄/IrO_x

System B: Carbon cloth/2.0 M H₂SO₄ 0.36 M V₂(SO₄)₃/Nafion/1.0 M H₂SO₄ 0.10 M Ce³⁺/Pt

System C: Carbon cloth/2.0 M H₂SO₄ 0.36 M V₂(SO₄)₃/BPM/2.0 M KOH/Ni mesh

This hybrid solar-driven water-splitting system represents a proof-of-concept demonstration of a strategy²⁰⁻²¹ for decoupling HER and OER in which a (photo-)electrochemical process is followed by a chemical process, separated in space and time, to produce hydrogen. In traditional PEC systems, generation of pressurized hydrogen over large area can be challenging due to issues associated with light management, reactant/product flows, *etc.* This hybrid system also enables the (photo-)electrochemical pressurization of hydrogen, using the vanadium redox couple as a mediator to store pressurized hydrogen in a liquid electrolyte. A similar concept has been reported previously using a two-electron, two-proton mediator, silicotungstic acid, for hydrogen generation.¹⁸ In contrast, the hybrid system described herein additionally utilized a bipolar membrane to mitigate the use of precious materials, such as Pt, Ir or Ru, for the water-oxidation reaction. In a two-step electrolysis system, in which the water-splitting reaction is effected in two physically distinct, separate electrochemical cells using redox species or redox electrodes,^{14-15, 17-}

1
2
3
4 ¹⁹ the hybrid approach demonstrated herein is likely to have lower capital costs because only one
5
6 electrolysis unit, and associate balance of systems, is required.
7
8
9

10
11 To demonstrate the capability of this system to produce spatially and temporally separated streams
12 of O₂(g) and H₂(g), the V^{3+/2+}(aq,H₂SO₄)|KOH(aq) cell with a 6.0 cm² electrode area was
13
14 connected in series with a 16% efficient, 13.1 cm² polycrystalline photovoltaic module attached to
15
16 a solar tracker, and the whole apparatus was tested outdoors (see Fig. S3 for picture of the outdoor
17
18 setup). Fig. 4a shows the illumination intensity (blue) and system current (black) for operation
19
20 during a day. For the first ~4.5 h, the photocurrent fluctuated around 73 mA, while the illumination
21
22 intensity fluctuated around 95 mW cm⁻². The fluctuations in the photocurrent matched
23
24 corresponding fluctuations in illumination intensity that were produced by environmental factors.
25
26 Between 14:17 and 15:47, a wind-blown tree caused extreme variability in the illumination
27
28 intensity, decreasing it from 95 to ~5 to mW cm⁻², and consequently producing a reduction in the
29
30 photocurrent from 69 mA to 5.0 mA. Cloud-cover between 16:45 to 17:00 caused the illumination
31
32 intensity to drop to ~5 mW cm⁻² and the photocurrent to drop to ~5.0 mA. After 17:17, a building
33
34 blocked the photovoltaic module from illumination by direct sunlight, so the illumination intensity
35
36 decreased to < 3 mW cm⁻², causing the current to decrease to < 3.0 mA. Fig. 4b overlays the
37
38 polarization behavior of the stand-alone V^{3+/2+}(aq,H₂SO₄)|KOH(aq) cell with the current density
39
40 vs. voltage (*J-V*) behavior of the photovoltaic module at various points in the day. As the V^{3+/2+}
41
42 solution was charged during the outdoor measurements, the polarization data shifted to higher
43
44 overpotentials and lower current densities, in accordance with the Nernst equation (Equation 5).
45
46
47
48
49
50
51
52
53
54
55
56
57
58
59
60

1
2
3
4 Shifts in the J - V and polarization behavior together caused the photocurrent to vary during
5
6 operation. After charging to 85% capacity, the entire 50 mL of catholyte was discharged with
7
8 Mo_2C , producing $\text{H}_2(\text{g})$ at 80% overall faradaic efficiency based on the total charge passed. The
9
10 discharged solution was then filtered with successively smaller filters, and the solution was reused
11
12 in the system. After the reused solution was charged to 86% capacity, the whole solution was
13
14 discharged, and produced $\text{H}_2(\text{g})$ at 78% overall faradaic efficiency based on the total charge passed
15
16 in the second $\text{V}^{3+/2+}$ charging process. In this second charging step, the presence of Mo_2C particles
17
18 $< 0.2 \mu\text{m}$ in size catalyzed the parasitic HER side reaction during charging, leading to a small drop
19
20 in efficiency in the reused catholyte. Increases in the catalyst size, or using an additional smaller
21
22 filter, would likely be beneficial to recycling the system. Consistently, charging a fresh vanadium
23
24 solution to 66% capacity yielded $\text{H}_2(\text{g})$ at 84% overall faradaic efficiency based on the total charge
25
26 passed in this first new charging cycle.
27
28
29
30
31
32
33
34
35
36
37

38 Two efficiency values, a diurnal averaged STH conversion efficiency, $\eta_{diurnal}$, and an average
39
40 STH conversion efficiency during daylight operation, $\eta_{operating}$, were used to evaluate the
41
42 performance of the PV-coupled hybrid device. $\eta_{diurnal}$ was defined as $\frac{LVH_{\text{H}_2}m_{\text{H}_2}}{(DNI_{diurnal} + DHI_{diurnal})A_{PV}}$, and
43
44 $\eta_{operating}$ was defined as $\frac{LVH_{\text{H}_2}m_{\text{H}_2}}{(DNI_{operating} + DHI_{operating})A_{PV}}$, in which LVH_{H_2} is the lower heating value of
45
46 hydrogen, m_{H_2} is the mass of hydrogen collected from the vanadium discharge reaction, A_{PV} is
47
48 the area of the photovoltaic module, $DNI_{diurnal}$ and $DNI_{operating}$ are the direct normal
49
50 irradiance integrated over a diurnal cycle and operating cycle, respectively, and $DHI_{diurnal}$ and
51
52 $DHI_{operating}$ are the direct horizontal irradiance integrated over a diurnal cycle and operating
53
54
55
56
57
58
59
60

1
2
3
4 cycle, respectively. By collecting the produced $\text{H}_2(\text{g})$ at night, $\eta_{diurnal} = 3.7\%$ and $\eta_{operating} =$
5
6
7 5.8% were obtained. PV modules with higher conversion efficiencies can further improve the
8
9 overall efficiency of this hybrid device, provided that the operating voltage of the module is $\sim 2.2-$
10
11 2.3 V, to maintain the desired cathode operating potential.

12
13
14
15
16
17 While the demonstration unit contained two discreet components: a PV cell and an electrochemical
18
19 reactor with the dark electrodes operating at current densities relevant to the solar photon flux, a
20
21 fully integrated hybrid device can be envisioned and constructed using many of the design
22
23 principles in integrated PEC water-splitting reactors.³⁸⁻³⁹ The further development and potential
24
25 deployment of such hybrid devices will likely primarily be in distributed applications and in places
26
27 where electric grids and electrical transmission are not available. In the distributed applications,
28
29 the operating current density of the catalysts and dark electrodes will be $\sim 10 \text{ mA cm}^{-2}$ as driven
30
31 by unconcentrated sunlight, hence the system described herein captures the key performance
32
33 metrics and characteristics of such a device. In addition, the Mo_2C powder used in this study could
34
35 be replaced with high surface area, porous medium to eliminate the filtering process, and the
36
37 required catalyst loading for the discharging process is relatively low for scalability of this concept.
38
39 For instance, without any optimization of the Mo_2C loading, to completely discharge the vanadium
40
41 electrolyte from a relatively large photoactive device (100 cm^2 active area, 10% STH conversion
42
43 efficiency, $7 \text{ kWh/m}^2/\text{day}$ solar insolation) under operation during the day, only 5 g of Mo_2C
44
45 catalyst will be needed to generate the hydrogen within 30 minutes during the night.
46
47
48
49
50
51
52
53
54
55
56
57
58
59
60

1
2
3
4 In summary, a proof-of-concept, hybrid solar-driven water-splitting device was demonstrated that
5
6 produces $O_2(g)$ in the daylight and produces $H_2(g)$ on demand at an elevated pressure. Instead of
7
8 transporting high pressure H_2 over a large area in a traditional solar-driven water-splitting device
9
10 that produces H_2 and O_2 simultaneously under illumination, the bipolar membrane-based hybrid
11
12 device stores the renewable electrons and protons temporarily (daily, weekly or even seasonally)
13
14 in the liquid form, *e.g.*, vanadium-based redox couples, which can be transported readily into a
15
16 centralized reactor for production of H_2 as desired. The “solar-charged” vanadium redox couples
17
18 could also be used in parallel with short-term electricity storage in the grid or longer-term fuel
19
20 production in conjunction with further reduction reactions, including CO_2 reduction or biomass
21
22 upgrades. The approach is complementary to other approaches that are being developed to
23
24 decouple the production of $H_2(g)$ and $O_2(g)$ in a water-splitting process, each of which has unique
25
26 advantages and disadvantages from a complexity, cost and safety perspective in laboratory-sized
27
28 demonstration systems in their use of simple *vs.* bipolar membranes, single *vs.* dual
29
30 electrochemical cells, earth-abundant *vs.* precious metal electrocatalysts, *etc.* The hybrid device
31
32 described herein thus provides additional possible design spaces for implementation of a
33
34 hydrogen-based “solar refinery”.
35
36
37
38
39
40
41
42
43
44
45
46
47
48
49
50
51
52
53
54
55
56
57
58
59
60

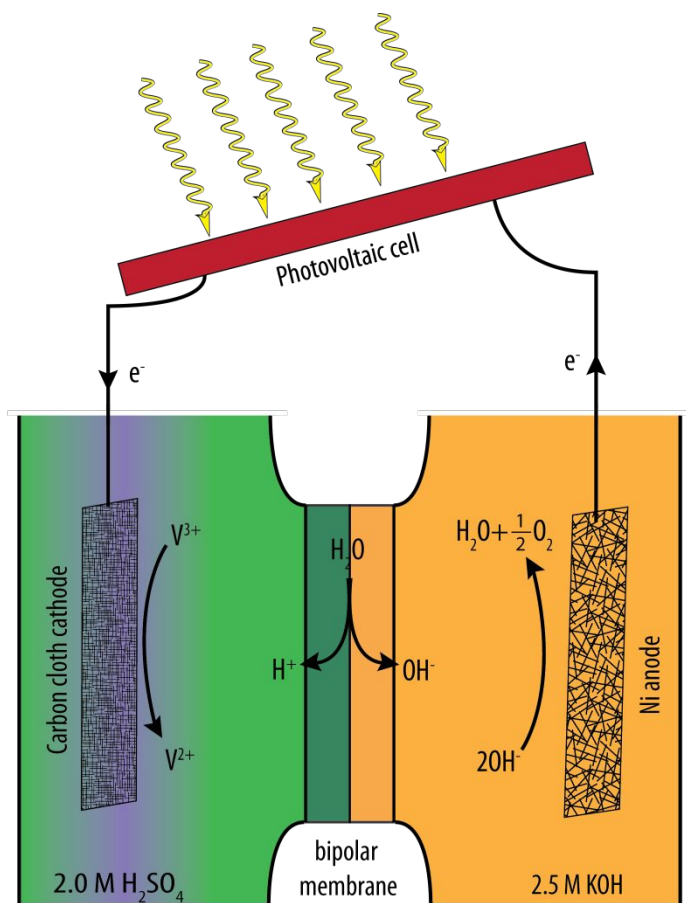


Figure 1. Schematic illustration of a solar-driven $V^{3+}/V^{2+}(aq, H_2SO_4)|KOH(aq)$ cell in which a photovoltaic module generates energetic electrons and holes, a carbon cloth cathode effects vanadium reduction in 2.0 M $H_2SO_4(aq)$, a Ni mesh anode oxidizes water to $O_2(g)$ in 2.5 M $KOH(aq)$, and a bipolar membrane sustains the pH differential between the cathode and anode chambers.

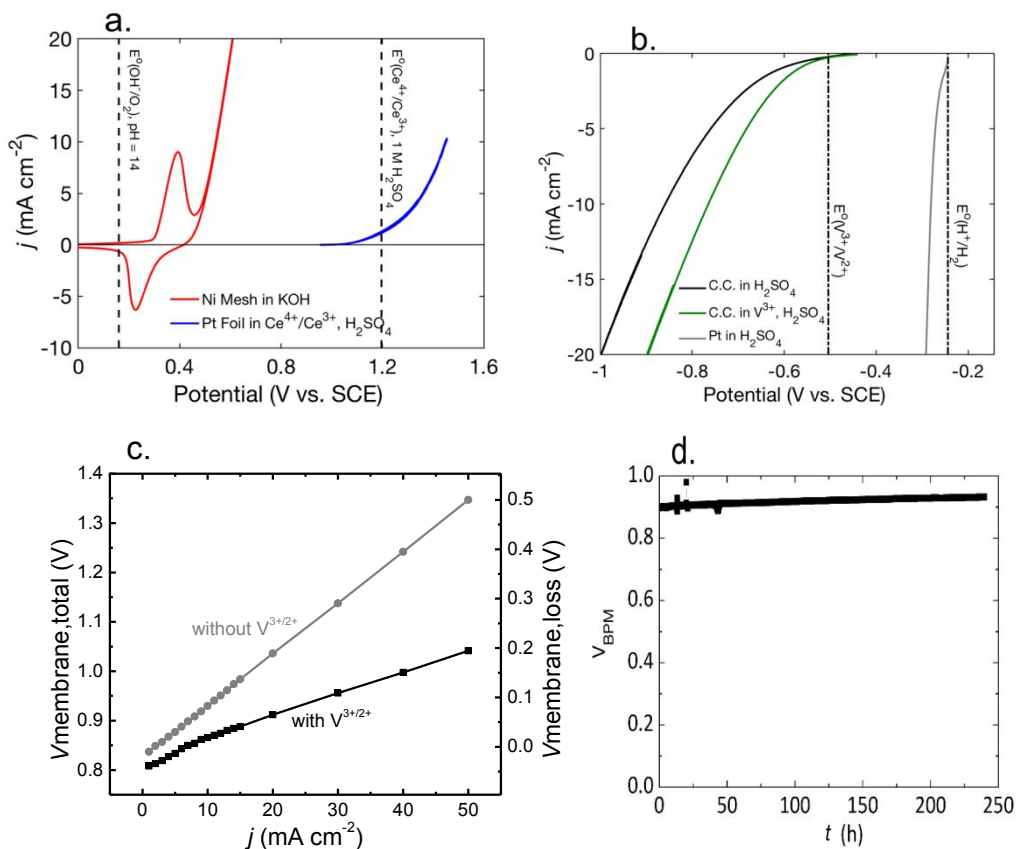


Figure 2. (a) Voltammetry of a Ni mesh (6.0 cm² geometric area) in 2.5 M KOH(aq) (red) and Pt foil (0.12 cm² area) in Ce⁴⁺/Ce³⁺, 1.0 M H₂SO₄(aq) (blue). (b) Voltammetry of a carbon cloth in 2.0 M H₂SO₄ (black) as well as of carbon cloth (6.0 cm² geometric area) in 0.36 M V³⁺, 2.0 M H₂SO₄(aq) (green). For comparison, voltammetry of Pt in 1.0 M H₂SO₄(aq) (grey) is shown.⁴⁰⁻⁴¹ (c) Measured membrane voltage, and voltage loss with (black squares) and without (grey circles) the presence of vanadium species, as a function of the current density normalized to the bipolar membrane. The cell configuration was 2.0 M H₂SO₄(aq) (pH = -0.16) with or without V³⁺/V²⁺/BPM/KOH(aq) (pH = 14.21). (d) Bipolar membrane voltage as a function of time, with the current density across the bipolar membrane maintained at 10 mA cm⁻². The BPM, cathode and anode each had a geometric surface area of 6.0 cm².

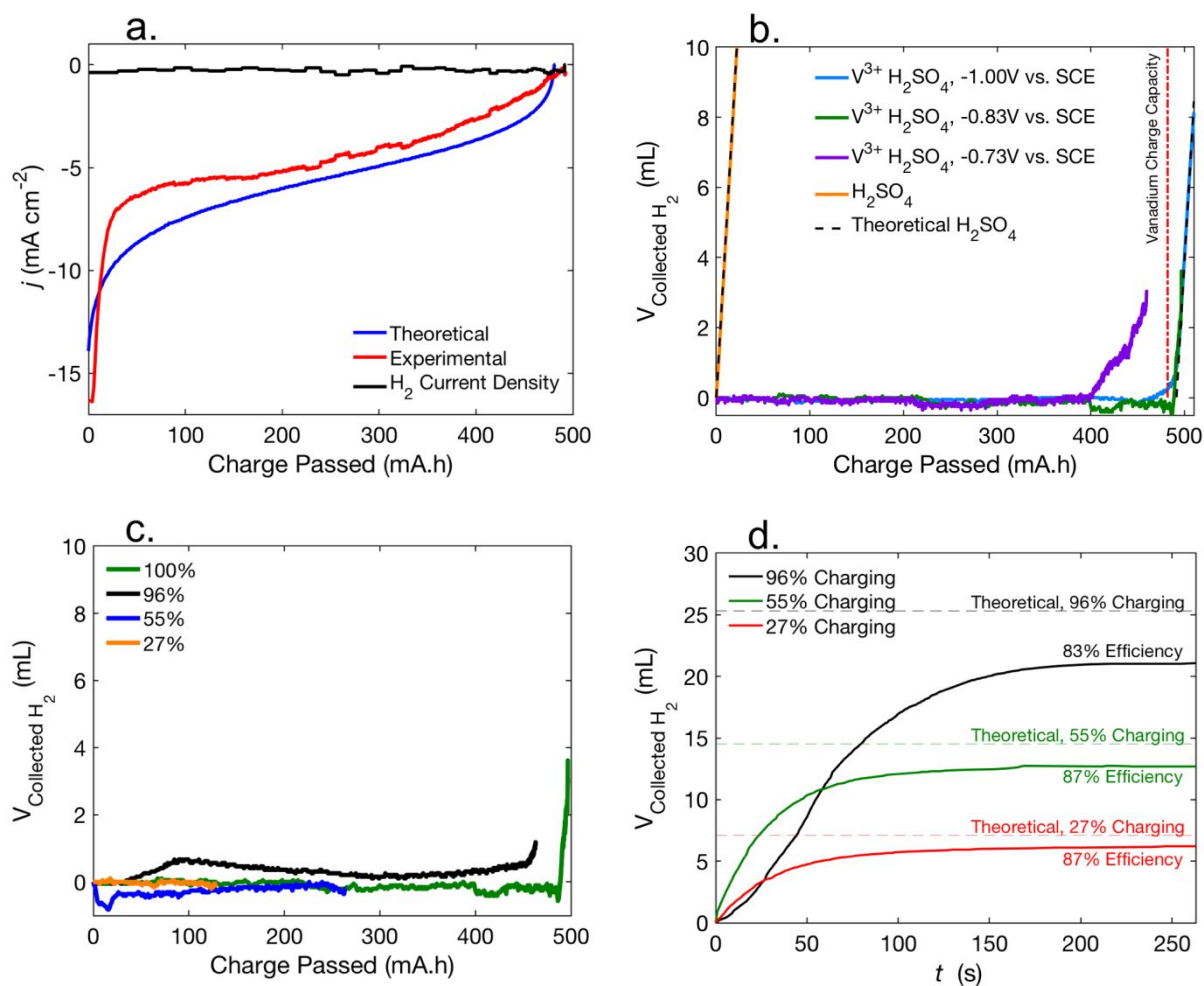


Figure 3. (a) Partial current density for the reduction of 0.36 M V³⁺ in 2.0 M H₂SO₄(aq) at -830 mV (*vs.* SCE) (red), partial current density for production of H₂(g) (black), and the theoretical current density determined by the Nernst equation, accounting for the 10 mA-h passed to the solution during the voltammetry (blue). (b) Measured H₂(g) collection during cell operation for 2.0 M H₂SO₄ (aq) (orange), 0.36 M V³⁺ in 2.0 M H₂SO₄(aq) at -1.00 V (blue), -0.830 V (green), and -0.73 V (purple) *vs.* SCE, respectively. The dotted black line shows the expected H₂ production volume in 2.0 M H₂SO₄ in the absence of vanadium species. (c) Hydrogen produced during runs of varying charge capacities at -830 mV *vs.* SCE. (d) Measured H₂(g) collection during reaction

1
2
3
4 of 6.0 mL of partially reduced 0.36 M V^{2+} , 2.0 M H_2SO_4 in the presence of the Mo_2C catalyst.
5
6
7
8
9
10
11
12
13
14
15
16
17
18
19
20
21
22
23
24
25
26
27
28
29
30
31
32
33
34
35
36
37
38
39
40
41
42
43
44
45
46
47
48
49
50
51
52
53
54
55
56
57
58
59
60

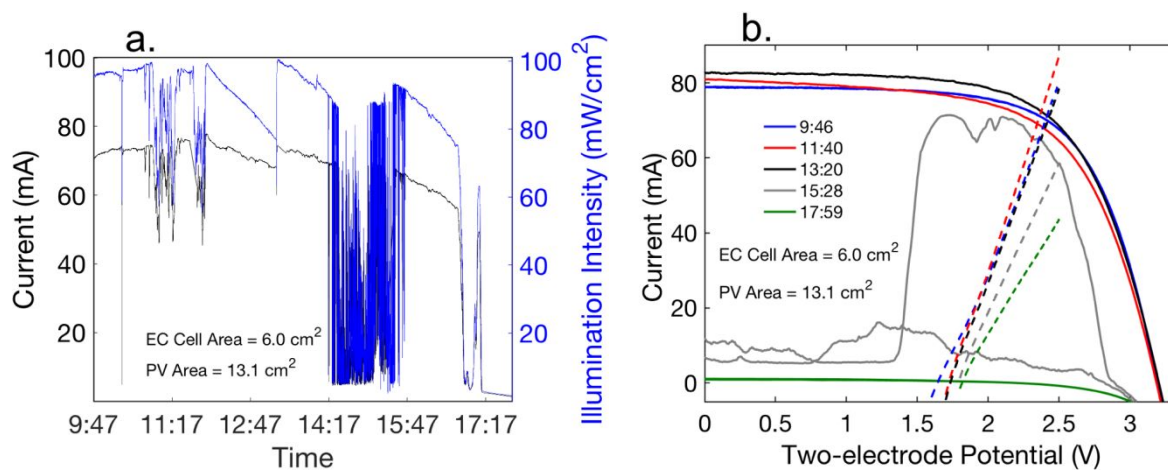


Figure 4. Outdoor measurements. (a) Current of the V^{3+/2+}(aq,H₂SO₄)|KOH(aq) cell coupled to a photovoltaic module (black), with the illumination intensity during cell operation measured by a photodiode (blue). (b) Overall polarization behavior for the photovoltaic module (solid lines) and for the V^{3+/2+}(aq,H₂SO₄)|KOH(aq) cell (dashed lines) during charging at times in the day.

ACKNOWLEDGMENT

This material is based upon work performed by the Joint Center for Artificial Photosynthesis, a DOE Energy Innovation Hub, supported through the Office of Science of the U.S. Department of Energy under Award Number DE-SC0004993, as well as the Gordon and Betty Moore Foundation.

The authors thank Caltech's SURF Board for a Summer Undergraduate Research Fellowship and acknowledge Caltech's Federal Work-Study program.

Supporting Information

The Supporting Information is available free of charge on the ACS Publications website at DOI: XXX, including: electrolyte and catalyst material information, electrochemical cell, electrochemical charging experiments, bipolar membrane measurement details, ion crossover measurements, outdoor charging experiments, and pressurization experiments.

REFERENCES

- (1) Haynes, W. M.; Lide, D. R.; Bruno, T. J., *Crc Handbook of Chemistry and Physics: A Ready-Reference Book Of Chemical and Physical Data*. CRC Press, Taylor & Francis Group: Boca Raton, Florida, USA, 2015.
- (2) Verlage, E.; Hu, S.; Liu, R.; Jones, R. J. R.; Sun, K.; Xiang, C.; Lewis, N. S.; Atwater, H. A. A Monolithically Integrated, Intrinsically Safe, 10% Efficient, Solar-Driven Water-Splitting System Based on Active, Stable Earth-Abundant Electrocatalysts in Conjunction with Tandem III-V Light Absorbers Protected By Amorphous TiO₂ Films. *Energy & Environ. Sci.* **2015**, *8* (11), 3166-3172.
- (3) Sun, K.; Liu, R.; Chen, Y.; Verlage, E.; Lewis, N. S.; Xiang, C. A Stabilized, Intrinsically Safe, 10% Efficient, Solar-Driven Water-Splitting Cell Incorporating Earth-Abundant Electrocatalysts with Steady-State pH Gradients and Product Separation Enabled by a Bipolar Membrane. *Adv. Energy Mater.* **2016**, *6* (13), 1600379.
- (4) Luo, J.; Vermaas, D. A.; Bi, D.; Hagfeldt, A.; Smith, W. A.; Grätzel, M. Bipolar Membrane-Assisted Solar Water Splitting in Optimal pH. *Adv. Energy Mater.* **2016**, *6*.
- (5) Luo, J.; Im, J.-H.; Mayer, M. T.; Schreier, M.; Nazeeruddin, M. K.; Park, N.-G.; Tilley, S. D.; Fan, H. J.; Grätzel, M. Water Photolysis at 12.3% Efficiency via Perovskite Photovoltaics and Earth-Abundant Catalysts. *Science* **2014**, *345* (6204), 1593-1596.
- (6) Wrighton, M. S.; Ellis, A. B.; Wolczanski, P. T.; Morse, D. L.; Abrahamson, H. B.; Ginley, D. S. Strontium Titanate Photoelectrodes. Efficient Photoassisted Electrolysis of Water at Zero Applied Potential. *J. Am. Chem. Soc.* **1976**, *98* (10), 2774-2779.

- 1
2
3
4 (7) Najjar, Y. S. H. Hydrogen Safety: The Road toward Green Technology. *Int. J. Hydrogen*
5
6 *Energy* **2013**, *38* (25), 10716-10728.
7
8
9 (8) Jin, J.; Walczak, K.; Singh, M. R.; Karp, C.; Lewis, N. S.; Xiang, C. An Experimental and
10
11 Modeling/Simulation-Based Evaluation of the Efficiency and Operational Performance
12
13 Characteristics of an Integrated, Membrane-Free, Neutral pH Solar-Driven Water-Splitting
14
15 System. *Energy & Environ. Sci.* **2014**, *7* (10), 3371-3380.
16
17
18
19 (9) Hashemi, S. M. H.; A. Modestino, M.; Psaltis, D. A Membrane-less Electrolyzer for Hydrogen
20
21 Production across the pH Scale. *Energy & Environ. Sci.* **2015**, *8* (7), 2003-2009.
22
23
24
25 (10) Hashemi, S. M. H.; Neuenschwander, M.; Hadikhani, P.; Modestino, M. A.; Psaltis, D.
26
27 Membrane-less Micro Fuel Cell Based on Two-Phase Flow. *J. Power Sources* **2017**, *348*, 212-
28
29 218.
30
31
32 (11) Rohland, B.; Eberle, K.; Ströbel, R.; Scholta, J.; Garche, J. Electrochemical Hydrogen
33
34 Compressor. *Electrochim. Acta* **1998**, *43* (24), 3841-3846.
35
36
37 (12) Ströbel, R.; Oszcipok, M.; Fasil, M.; Rohland, B.; Jörisen, L.; Garche, J. The
38
39 Compression of Hydrogen in an Electrochemical Cell Based on a Pe Fuel Cell Design. *J. Power*
40
41 *Sources* **2002**, *105* (2), 208-215.
42
43
44 (13) Collier, A.; Wang, H.; Zi Yuan, X.; Zhang, J.; Wilkinson, D. P. Degradation of Polymer
45
46 Electrolyte Membranes. *Int. J. Hydrogen Energy* **2006**, *31* (13), 1838-1854.
47
48
49 (14) Tang, H.; Peikang, S.; Jiang, S. P.; Wang, F.; Pan, M. A Degradation Study of Nafion
50
51 Proton Exchange Membrane of Pem Fuel Cells. *J. Power Sources* **2007**, *170* (1), 85-92.
52
53
54 (15) Chen, L.; Dong, X.; Wang, Y.; Xia, Y. Separating Hydrogen and Oxygen Evolution in
55
56
57
58
59
60

1
2
3
4 Alkaline Water Electrolysis Using Nickel Hydroxide. *Nat. Commun.* **2016**, *7*, 11741.

5
6 (16) Landman, A.; Dotan, H.; Shter, G. E.; Wullenkord, M.; Houaijia, A.; Maljusch, A.;
7
8 Grader, G. S.; Rothschild, A. Photoelectrochemical Water Splitting in Separate Oxygen and
9
10 Hydrogen Cells. *Nat. Mater.* **2017**, *16*, 646-651.

11
12 (17) Ma, Y. Y.; Dong, X. L.; Wang, Y. G.; Xia, Y. Y. Decoupling Hydrogen and Oxygen
13
14 Production in Acidic Water Electrolysis Using a Polytriphenylamine-Based Battery Electrode.
15
16
17
18
19 *Angew. Chem. Int. Ed.* **2018**, *57* (11), 2904-2908.

20
21 (18) Bloor, L. G.; Solarska, R.; Bienkowski, K.; Kulesza, P. J.; Augustynski, J.; Symes, M.
22
23 D.; Cronin, L. Solar-Driven Water Oxidation and Decoupled Hydrogen Production Mediated by
24
25 an Electron-Coupled-Proton Buffer. *J. Am. Chem. Soc.* **2016**, *138* (21), 6707-6710.

26
27 (19) Symes, M. D.; Cronin, L. Decoupling Hydrogen and Oxygen Evolution during
28
29 Electrolytic Water Splitting Using an Electron-Coupled-Proton Buffer. *Nat. Chem.* **2013**, *5* (5),
30
31
32
33
34
35 403-409.

36
37 (20) Rausch, B.; Symes, M. D.; Chisholm, G.; Cronin, L. Decoupled Catalytic Hydrogen
38
39 Evolution from a Molecular Metal Oxide Redox Mediator in Water Splitting. *Science* **2014**, *345*
40
41
42
43 (6202), 1326-1330.

44
45 (21) Amstutz, V.; Toghiani, K. E.; Powlesland, F.; Vrubel, H.; Comninellis, C.; Hu, X. L.;
46
47 Girault, H. H. Renewable Hydrogen Generation from a Dual-Circuit Redox Flow Battery. *Energy*
48
49
50
51 & *Environ. Sci.* **2014**, *7* (7), 2350-2358.

52
53 (22) McCrory, C. C. L.; Jung, S.; Ferrer, I. M.; Chatman, S. M.; Peters, J. C.; Jaramillo, T. F.
54
55
56 Benchmarking Hydrogen Evolving Reaction and Oxygen Evolving Reaction Electrocatalysts for
57
58

1
2
3
4 Solar Water Splitting Devices. *J. Am. Chem. Soc.* **2015**, *137* (13), 4347-4357.

5
6 (23) McCrory, C. C. L.; Jung, S.; Peters, J. C.; Jaramillo, T. F. Benchmarking Heterogeneous
7
8 Electrochemicals for the Oxygen Evolution Reaction. *J. Am. Chem. Soc.* **2013**, *135* (45), 16977-
9
10 16987.

11
12 (24) Sun, K.; Saadi, F. H.; Lichterman, M. F.; Hale, W. G.; Wang, H.-P.; Zhou, X.; Plymale,
13
14 N. T.; Omelchenko, S. T.; He, J.-H.; Papadantonakis, K. M., *et al.* Stable Solar-Driven Oxidation
15
16 of Water by Semiconducting Photoanodes Protected by Transparent Catalytic Nickel Oxide Films.
17
18 *Proc. Natl. Acad. Sci. U.S.A.* **2015**, *112* (12), 3612-3617.

19
20 (25) Sun, K.; McDowell, M. T.; Nielander, A. C.; Hu, S.; Shaner, M. R.; Yang, F.; Brunshwig,
21
22 B. S.; Lewis, N. S. Stable Solar-Driven Water Oxidation to O₂(g) by Ni-Oxide-Coated Silicon
23
24 Photoanodes. *J. Phys. Chem. Lett.* **2015**, *6* (4), 592-598.

25
26 (26) Zhou, X.; Liu, R.; Sun, K.; Friedrich, D.; McDowell, M. T.; Yang, F.; Omelchenko, S.
27
28 T.; Saadi, F. H.; Nielander, A. C.; Yalamanchili, S., *et al.* Interface Engineering of the
29
30 Photoelectrochemical Performance of Ni-Oxide-Coated n-Si Photoanodes by Atomic-Layer
31
32 Deposition of Ultrathin Films of Cobalt Oxide. *Energy & Environ. Sci.* **2015**, *8* (9), 2644-2649.

33
34 (27) Kenney, M. J.; Gong, M.; Li, Y.; Wu, J. Z.; Feng, J.; Lanza, M.; Dai, H. High-
35
36 Performance Silicon Photoanodes Passivated with Ultrathin Nickel Films for Water Oxidation.
37
38 *Science* **2013**, *342* (6160), 836-40.

39
40 (28) Walter, M. G.; Warren, E. L.; McKone, J. R.; Boettcher, S. W.; Mi, Q.; Santori, E. A.;
41
42 Lewis, N. S. Solar Water Splitting Cells. *Chem. Rev.* **2010**, *110* (11), 6446-6473.

43
44 (29) Jiang, C.; Moniz, S. J. A.; Wang, A.; Zhang, T.; Tang, J. Photoelectrochemical Devices
45
46
47
48
49
50
51
52
53
54
55

1
2
3
4 for Solar Water Splitting - Materials and Challenges. *Chem. Soc. Rev.* **2017**, *46* (15), 4645-4660.

5
6 (30) Sivula, K.; van de Krol, R. Semiconducting Materials for Photoelectrochemical Energy
7
8 Conversion. *Nat. Rev. Mater.* **2016**, *1*, 15010.

9
10 (31) Heller, A.; Miller, B.; Thiel, F. A. 11.5% Solar Conversion Efficiency in the
11
12 Photocathodically Protected $p\text{-Inp}/\text{V}^{3+}\text{-V}^{2+}$ - HCl/C Semiconductor Liquid Junction Cell. *Appl.*
13
14 *Phys. Lett.* **1981**, *38* (4), 282-284.

15
16 (32) Reiter, R. S.; White, W.; Ardo, S. Communication—Electrochemical Characterization of
17
18 Commercial Bipolar Membranes under Electrolyte Conditions Relevant to Solar Fuels
19
20 Technologies. *J. Electrochem. Soc.* **2016**, *163* (4), H3132-H3134.

21
22 (33) Vermaas, D. A.; Wiegman, S.; Nagaki, T.; Smith, W. A. Ion Transport Mechanisms in
23
24 Bipolar Membranes for (Photo)electrochemical Water Splitting. *Sustainable Energy Fuels* **2018**,
25
26 *2* (9), 2006-2015.

27
28 (34) Vargas-Barbosa, N. M.; Geise, G. M.; Hickner, M. A.; Mallouk, T. E. Assessing the
29
30 Utility of Bipolar Membranes for use in Photoelectrochemical Water-Splitting Cells.
31
32 *ChemSusChem* **2014**, *7* (11), 3017-3020.

33
34 (35) Zhou, X.; Liu, R.; Sun, K.; Chen, Y.; Verlage, E.; Francis, S. A.; Lewis, N. S.; Xiang, C.
35
36 Solar-Driven Reduction Of 1 atm of CO_2 to Formate at 10% Energy-Conversion Efficiency by
37
38 Use of a TiO_2 -Protected III–V Tandem Photoanode in Conjunction with a Bipolar Membrane and
39
40 a Pd/C Cathode. *ACS Energy Lett.* **2016**, *1* (4), 764-770.

41
42 (36) Yan, Z.; Zhu, L.; Li, Y. C.; Wycisk, R. J.; Pintauro, P. N.; Hickner, M. A.; Mallouk, T.
43
44 E. The Balance of Electric Field and Interfacial Catalysis in Promoting Water Dissociation in
45
46
47
48
49
50
51
52
53
54
55
56
57
58
59
60

1
2
3
4 Bipolar Membranes. *Energy & Environ. Sci.* **2018**, *11* (8), 2235-2245.

5
6 (37) Vermaas, D. A.; Sassenburg, M.; Smith, W. A. Photo-Assisted Water Splitting with
7
8 Bipolar Membrane Induced pH Gradients for Practical Solar Fuel Devices. *Journal of Materials*
9
10
11
12 *Chemistry A* **2015**, *3* (38), 19556-19562.

13
14 (38) Haussener, S.; Xiang, C. X.; Spurgeon, J. M.; Ardo, S.; Lewis, N. S.; Weber, A. Z.
15
16 Modeling, Simulation, and Design Criteria for Photoelectrochemical Water-Splitting Systems.
17
18
19
20
21 *Energy & Environ. Sci.* **2012**, *5* (12), 9922-9935.

22 (39) Xiang, C.; Weber, A. Z.; Ardo, S.; Berger, A.; Chen, Y.; Coridan, R.; Fontaine, K. T.;
23
24 Haussener, S.; Hu, S.; Liu, R., *et al.* Modeling, Simulation, and Implementation of Solar-Driven
25
26
27
28
29 Water-Splitting Devices. *Angew. Chem. Int. Ed.* **2016**, *55* (42), 12974-12988.

30 (40) Saadi, F. H.; Carim, A. I.; Drisdell, W. S.; Gul, S.; Baricuatro, J. H.; Yano, J.; Soriaga,
31
32
33
34
35
36
37 M. P.; Lewis, N. S. Operando Spectroscopic Analysis of Cop Films Electrocatalyzing the
38
39
40
41
42
43
44
45
46
47
48
49
50
51
52
53
54
55
56
57
58
59
60 Hydrogen-Evolution Reaction. *J. Am. Chem. Soc.* **2017**, *139* (37), 12927-12930.

(41) Saadi, F. H.; Carim, A. I.; Verlage, E.; Hemminger, J. C.; Lewis, N. S.; Soriaga, M. P.
Cop as an Acid-Stable Active Electrocatalyst for the Hydrogen-Evolution Reaction:
Electrochemical Synthesis, Interfacial Characterization and Performance Evaluation. *J. Phys.*
Chem. C **2014**, *118* (50), 29294-29300.